A simulation study of steric effects on the anodic dissolution at high current densities

Köhn, Christoph; Laethem, Dries; Deconinck, Johan; Hubin, Annick

Published in:
Materials and Corrosion

Link to article, DOI:
10.1002/maco.202012051

Publication date:
2021

Document Version
Publisher's PDF, also known as Version of record

Received: 3 September 2020 | Revised: 8 November 2020 | Accepted: 27 November 2020

DOI: 10.1002/maco.202012051

ARTICLE

Materials and Corrosion

A simulation study of steric effects on the anodic dissolution at high current densities

Christoph Köhn[1,2] | Dries van Laethem[2] | Johan Deconinck[2] | Annick Hubin[2]

[1]National Space Institute (DTU Space), Technical University of Denmark, Lyngby, Denmark

[2]Research Group Electrochemical and Surface Engineering, (SURF), Vrije Universiteit Brussel, Brussels, Belgium

Correspondence
Christoph Köhn, National Space Institute (DTU Space), Technical University of Denmark, Elektrovej 328, 2800 Kgs Lyngby, Denmark.
Email: koehn@space.dtu.dk

Abstract

Electrochemical machining (ECM) and electropolishing are examples of anodic dissolution used in a wide variety of applications. Proper simulations of ECM require the establishment of a so-called gel layer of liquid metal salt, responsible for the depletion of water close to the surface such that the oxygen evolution is reduced. However, this effect is neglected in many simulation efforts, although it is significant to improve the accuracy of the machining process. Some authors consider this effect by an engineered "water-repelling" function that depends on the local metal ion concentration. As an alternative, we discuss the theoretical description and the implementation of modified Poisson–Nernst–Planck equations taking into account expressions in which each ion has its own maximum concentration and corresponding steric limit. We investigate a basic system of water, sodium chloride, and iron ions. Simulations pending on the local metal ion concentration for current densities show that the modified model works; steric effects become important for large current densities and the formation of a resistive gel layer is responsible for the reduction of water at the electrode. We observe that the electrostatic potential resulting from space charge effects is not affected by implementing the different species sizes. Further research is needed to explore the applicability of industrial simulation tools.

KEYWORDS

anodic dissolution, electrochemical machining, electrochemical simulations, high current densities, steric effects

1 | INTRODUCTION

Anodic dissolution is related to various processes at different current densities. Among these, there is the growth stadium of pitting corrosion for current densities in the order of 10 mA cm^{-2},[1] crevice corrosion for tens and hundreds of mA cm^{-2}, electrochemical polishing for hundreds of mA cm^{-2},[2] and electrochemical machining (ECM) for even higher current densities.[3]

ECM that can be interpreted as goal-directed corrosion is an alternative machining technique, where the anode is used as the workpiece and the cathode is utilized as the work tool. The advantage of ECM is that it works far away from thermodynamic equilibrium (10–300 A cm^{-2}) and that there is no abrasive wear on the work tool nor stress on the workpiece since the workpiece and tool do not touch each other.[4] A major example is the tooling of very hard and complex-shaped turbine blades made of nickel superalloys.

ECM is based on anodic dissolution, which makes it suitable to study the dissolution of various materials at high current densities; see, for example, Schneider et al.,[5–7] and references therein. Beyond that, ECM is used in a variety of applications, such as for surface polishing,[8–11] stainless steel machining microelements with ultrashort voltage pulses,[12,13] or for the machining of three-dimensional (3D) microstructures.[14–17]

In view of obtaining the right geometry of the workpiece, the so-called copying accuracy of the process is of utmost relevance. Cathode shape, but also fluid flow, gas evolution, temperature distribution, and electrode processes have an effect. So, simulations can speed up the production process and reduce the costs of testing. The most advanced ECM simulations are based on the dilute solution model (DSM). However, simulations, described through the Poisson–Nernst–Planck (PNP) equations, yield unrealistic high concentrations of dissolving metal cations accumulating in the vicinity of the anode.[18] Such ions recombine from hydrated metal salts that reach concentrations that are far beyond saturation limits because ion–ion interactions and steric effects are commonly neglected at high current densities. In addition, the DSM cannot correctly describe the reduction of the water concentration in the vicinity of the anode, which reduces the oxygen evolution and increases the metal removal efficiency at higher current densities.[19]

Solving the DSM equations with or without steric effects is not only limited to electromechanical machining simulations. As an example, Dykstra et al.[20] simulated the ion transport in bioelectrochemical systems, which are electrochemical cells that use microorganisms as catalysators.[21,22] They include the diffusional and electric forces of ions and focus on the motion and evaporation of ammonia in such systems. They find that ammonia diffuses back from the cathode into the anode chamber because of the ion exchange at the membrane placed between the anode and cathode.

We mentioned the importance of the presence of water at the anode. A practical and simple way to deal with this at increased current densities in ECM simulations is the usage of "water-repelling" functions[23,24] that depend on the local metal ion concentration. This implies that a kind of self-enhancing process is obtained from a given current density on. At the same local current density, the absence of water results in higher concentrations of metal ions that further reduce the water concentration. Such simulations are 2D and 3D in their nature and include gas flow and heat reactions[25,26] but ignore the steric effect of all involved species, which shows the need to combine simulations with steric effects.

For a better understanding of the fundamental principles of the ECM process, we require an extension of the dilute solution theory. In 2007, Kilic et al.[27,28] presented the modified Poisson–Nernst–Planck (MPNP) equations that are based on modified electrochemical potentials. The theory was developed for a solvent with two species having the same steric limit $c_{\max} = 1/a^3$, where a^3 is the typical spacing near a highly charged surface. They apply their theory to describe the charging of electric double-layer capacitors in a parallel plate cell. Lin and Eisenberg[29] had a similar approach based on modifying the Lennard–Jones potential.

We here extend this approach for an arbitrary number of species, each with their own steric limit, and for high current densities making it necessary to take into account water repulsion. Besides the two requirements for the dilute solution theory, that is, mass conservation and electroneutrality, a new equilibrium condition must assure that the total specific volume is one; additionally, chemical reactions need to be expressed in activities. We call this the steric effect model (SEM) and we expect to see the role of steric effects and, at least qualitatively, explain some important aspects of a gel layer of liquid metal salt that is formed during ECM, which thus serves as a role model on how steric effects influence anodic dissolution at high current densities.

The article is structured as follows: In Section 2, we present the theory. We describe the numerical implementation and apply this theory to a 1D geometry. In Section 3, we present and discuss our results and compare the differences between the DSM and SEM equations applied to the ECM of metal in a salt solution. We finally conclude in Section 4.

2 | MODELING

2.1 | The modified PNP equations

2.1.1 | Electrochemical potential

We can apply statistical mechanics, similar to the calculations performed in Kralj-Iglič and Iglič,[30] to calculate the configurational entropy

$$S = k_B \ln \Omega, \tag{1}$$

and subsequently the electrochemical potential through

$$\mu_k = -T \frac{\partial S}{\partial N_k} \Big|_{N_{j \neq k}}, \tag{2}$$

from the thermodynamic probability for negligible enthalpy,[31] where $k_B \approx 1.38 \times 10^{-23}\,\mathrm{J\,K^{-1}}$ is Boltzmann's constant and T temperature. Let us suppose a lattice of 1D Lagrange elements of second-order with N sites, each filled with a particle from species j. When there are n

different kinds of species, the amount of different possible configurations equals

$$\Omega = \frac{N!}{\prod_{j=1}^{n} N_j!}, \tag{3}$$

which strictly speaking is only valid if all particles had the same volume, but which we take as a first approximation for our discussion below. The nodal spacing, as a 1D equivalent of the lattice volume, is not determined by the maximum package density but solely by the convergence of the finite element simulation. Furthermore, we make three assumptions to simplify this expression:

1. The factorials can be simplified by using Stirling's approximation[32]

$$\Omega \approx N \ln(N) - \sum_{j=1}^{n} N_j \ln(N_j). \tag{4}$$

2. Every lattice site is filled, that is,

$$N = \sum_{j=1}^{n} N_j. \tag{5}$$

3. The complete lattice has a volume V and each particle of species j has a volume v_j; thus, we can eliminate one of the species through

$$V = \sum_{j=1}^{n} v_j N_j, \tag{6}$$

$$N_n = \frac{1}{v_n}\left(V - \sum_{j=1}^{n-1} v_j N_j\right). \tag{7}$$

Here and in the rest of the article, the subscript n refers to the solvent of the solution.

When assuming that N_j can vary in space and time, we can define a local concentration field

$$c_j = \lim_{V \to 0} \frac{N_j}{N}. \tag{8}$$

Similarly, we need to transform the thermodynamic probability into a local quantity

$$\omega = \lim_{V \to 0} \frac{\Omega}{N}, \tag{9}$$

where we introduce a function ω, which is continuous in space and time. Finally, when eliminating species n and assuming that the particle volumes of all species are equal to v, we insert the local probability into (1), which allows us to calculate the chemical potential (2) of species i

$$\tilde{\mu}_{i \neq n} = RT \log\left(\frac{c_i}{\frac{1}{vN_a} - \sum_{j=1}^{n-1} c_j}\right) = RT \log\left(\frac{c_i}{c_n}\right), \tag{10}$$

where $N_a \approx 6.022 \times 10^{23}\,\mathrm{mol}^{-1}$ is Avogadro's constant and $R \approx 8.314\,\mathrm{J\,mol^{-1}\,K^{-1}}$ the universal gas constant. This expression is equivalent to eq. (24) in Kilic et al. [27] and eq. (11) in Kilic et al.[28] for two different species of equal size. Finally, the sum of the chemical potential (10) and the electric potential yields the electrochemical potential

$$\mu_i = RT \log\left(\frac{c_i}{c_n}\right) + z_i F U, \tag{11}$$

where $F \approx 96{,}485.33\,\mathrm{As\,mol^{-1}}$ is Faraday's constant and

$$c_n = \frac{1}{vN_a} - \sum_{j=1}^{n-1} c_j \tag{12}$$

is the concentration of the solvent.

2.1.2 | Mass flux

If we assume constant temperature and linear nonequilibrium thermodynamics, the mass flux of species i is given by

$$N_{i,i \neq n} = -\frac{D_i c_i}{RT} \nabla \mu_i, \tag{13}$$

$$= -D_i \nabla c_i - z_i D_i c_i \frac{F}{RT} \nabla U + D_i \frac{c_i}{c_n} \nabla c_n, \tag{14}$$

where we have inserted (11) into (13), where D_i is the diffusion coefficient of species i. The first two terms in (14) are the standard diffusion and migration terms from the DSM, while the last term (in boldface) represents the influence of steric effects. In the presence of n different species, the system can thus be described by n equations: $(n-1)$ mass balance equations combined with the Poisson equation for the electrostatic potential.

2.1.3 | Homogeneous reactions

Modifying the electrochemical potential as in (11) requires changing the expressions for homogeneous chemical reactions. If we assume a reaction such as

$$\sum_r \nu_r \mathrm{species}_r \rightleftharpoons \sum_p \nu_p \mathrm{species}_p, \tag{15}$$

this reaction is at equilibrium when the change in the Gibbs-free energy equals zero, that is,

$$\sum_r \nu_r \mu_r = \sum_p \nu_p \mu_p. \tag{16}$$

Inserting (11) into (16), the equilibrium condition can thus be expressed as

$$\frac{\prod_p \left(\frac{c_p}{c_n}\right)^{\nu_p}}{\prod_r \left(\frac{c_r}{c_n}\right)^{\nu_r}} = K = e^{-\frac{\Delta G^0}{RT}}, \tag{17}$$

where G^0 is the standard free energy change for the reaction. This relation explicitly describes how the ion equilibria are modified with finite volume effects.

Finally, using the assumption of identical volumes for each particle, Table 1 summarizes the differences between the DSM and the SEM.

2.2 | Setup of the model

We here apply the introduced model, including steric effects, to a system describing the ECM process. Therefore, we include water, sodium chloride, hydrated iron chloride, as well as the corresponding ions. Throughout this article, we refer to iron as "Me" since our analysis is not limited to iron but applicable to a variety of hydrated metal chlorides. Since we focus on the fundamental aspects of such a model, we limit ourselves to a 1D problem with the domain size $X = 40\,\mu\text{m}$, as depicted in Figure 1.

Using the mass flux (14), the governing equations for the steric effects model in 1D without reaction terms are thus for each species i (except for the solvent n)

$$0 = -\frac{d}{dx}\left(D_i \frac{d}{dx} c_i\right) - \frac{d}{dx}\left(M_i \frac{d}{dx} U\right) + \frac{d}{dx}\left(D_{\mu,i} \frac{c_i}{c_n} \frac{d}{dx} c_n\right), \tag{18}$$

together with the Poisson equation for the electrostatic potential U

$$0 = \frac{d^2}{dx^2} U + \varrho, \tag{19}$$

where

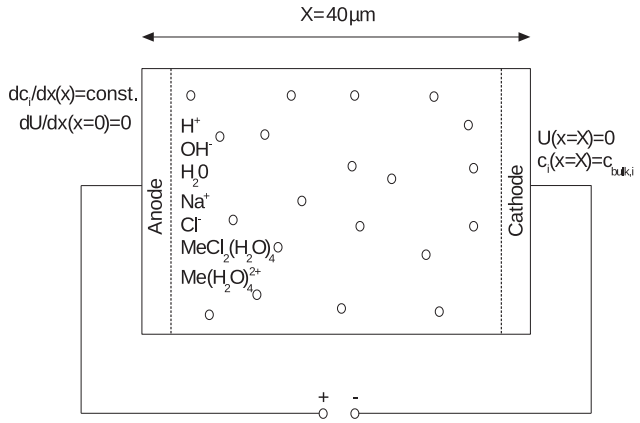

FIGURE 1 Sketch of the simulation

$$\varrho = \frac{F}{\epsilon_r}\left(z_{H^+} c_{H^+} + z_{Me^{2+}} c_{Me^{2+}} + z_{Cl^-} c_{Cl^-} + z_{Na^+} c_{Na^+}\right) \tag{20}$$

describes the charge density with the electric charge z_i of species i with electric permittivity $\varepsilon_r \approx 10^{-9}\,\text{A s V}^{-1}\,\text{m}^{-1}$. Note that we are mainly interested in steady-state solutions and therefore did not conduct any time-depending, transient simulations. However, in principle, the extension of (18) to transient simulations where the boundary conditions change over time is possible; in such a case, we do not expect any overshoot or oscillatory phenomena, given the nature of the applied equations.

Note for comparison that the governing equation of the DSM is

$$0 = -\frac{d}{dx}\left(D_i \frac{d}{dx} c_i\right) - \frac{d}{dx}\left(M_i \frac{d}{dx} U\right), \tag{21}$$

which is Equation (18) without the steric effects.

To avoid solving for a flow field, an equivalent concentration-independent diffusion is introduced with a turbulent diffusion constant that increases rapidly with increasing distance from the wall [33]

$$D_i \to D_{\Lambda,i} = D_{\Lambda,0} \times \left(\frac{x}{\Lambda}\right)^4 + D_i \tag{22}$$

with $D_{\Lambda,0} = 10^{-9}\,\text{m}^2\,\text{s}^{-1}$ and with the distance $\Lambda = 2\,\mu\text{m}$ from where convection starts to dominate the flow; this

TABLE 1 Overview of the governing equations of the dilute solution model and of the steric effect model

	Dilute solution model	Steric effect model
Electrochemical potential	$\mu_i = RT \log(c_i) + z_i F U$	$\mu_i = RT \log\left(\frac{c_i}{c_n}\right) + z_i F U$ $c_n = \frac{1}{\nu N_a} - \sum_{j=1}^{n-1} c_j$
Mass flux	$\vec{N}_{i,i\neq n} = -D_i \nabla c_i - z_i D_i c_i \frac{F}{RT} \nabla U$	$\vec{N}_{i,i\neq n} = -D_i \nabla c_i - z_i D_i c_i \frac{F}{RT} \nabla U + D_i \frac{c_i}{c_n} \nabla c_n$
Reaction equilibrium	$\frac{\prod_p c_p^{\nu_p}}{\prod_r c_r^{\nu_r}} = K$	$\frac{\prod_p \left(\frac{c_p}{c_n}\right)^{\nu_p}}{\prod_r \left(\frac{c_r}{c_n}\right)^{\nu_r}} = K$

turbulent diffusion constant is then used to substitute the diffusion coefficient in Equations (18 and 21). Note that $D_{\Lambda,i}$ do not explicitly depend on the particle size.

Finally, for each species i, the migration coefficients are given through

$$M_i = \frac{D_i \cdot z_i \cdot F}{R \cdot T} c_i, \tag{23}$$

where we fix the ambient temperature to $T = 25°C$.

In addition to Equations (18) and (19), we impose the bulk concentrations of the different species at the boundaries as Dirichlet boundary conditions

$$c_i(x = X) = c_{\text{bulk},i}, \tag{24}$$

and we impose a zero reference value for the electrostatic potential:

$$U(x = X) = 0. \tag{25}$$

At the anode, metal is oxidized and subsequently hydrated by water:

$$\text{Me} \leftrightharpoons \text{Me}^{2+} + 2\text{e}^-, \tag{26}$$

$$\text{Me}^{2+} + 4\text{H}_2\text{O} \leftrightharpoons \text{Me}(\text{H}_2\text{O})_4^{2+}. \tag{27}$$

In this study, we assume that the hydration reaction (27) happens instantaneously. As a result, (26) and (27) can be combined to write a single electrode reaction:

$$\text{Me} + 4\text{H}_2\text{O} \leftrightharpoons \text{Me}(\text{H}_2\text{O})_4^{2+} + 2\text{e}^-. \tag{28}$$

For simplicity, we limit ourselves to the formation of tetraquo complexes for the simulations presented in this article. Although more sophisticated chemistry might be involved, this is already sufficient to demonstrate the influence of steric effects at high current densities.

Furthermore, we assume that the current at the electrode is carried only by diffusion and not by migration. Under these assumptions, the Neumann boundary conditions at the anode are:

$$\frac{dc_{\text{Me}(\text{H}_2\text{O})_4^{2+}}}{dx}(x = 0) = -\frac{j}{z_{\text{Me}(\text{H}_2\text{O})_4^{2+}} D_{\text{Me}(\text{H}_2\text{O})_4^{2+}} F}, \tag{29}$$

$$\frac{dc_{\text{H}_2\text{O}}}{dx}(x = 0) = -4\frac{D_{\text{Me}(\text{H}_2\text{O})_4^{2+}}}{D_{\text{H}_2\text{O}}} \frac{dc_{\text{Me}(\text{H}_2\text{O})_4^{2+}}}{dx}(x = 0), \tag{30}$$

$$\frac{dc_i}{dx}(x = 0) = 0, \forall\, i \neq \text{H}_2\text{O}, \text{Me}(\text{H}_2\text{O})_4^{2+}, \tag{31}$$

$$\frac{dU}{dx}(x = 0) = 0, \tag{32}$$

where j is the imposed current density controlling the motion of particles at the boundary.

TABLE 2 Input parameters of our setup

i	D_i [10^{-9} m^2 s^{-1}]	z_i	v_i [10^{-30} m^{-3}]	$c_{\text{bulk},i}$ [mol m^{-3}]
H^+	9.31	+1	1.73	10^{-4}
OH^-	5.26	−1	3.38	10^{-4}
H_2O	2.27	0	27.00	55.3×10^3
$MeCl_2(H_2O)_4$	12.40	0	186.00	1.0
$Me(H_2O)_4^{2+}$	0.12	+2	11.00	10^{-6}
Cl^-	1.90	−1	37.30	2941.00
Na^+	1.33	+1	12.50	2941.00

The values for the diffusion coefficients D_i, the charges z_i, the volumes v_i, and the bulk concentrations $c_{\text{bulk},i}$ are summarized in Table 2.[18,34]

All equations are solved using the finite element method on a grid with 4000 nodes. The implementation is performed in the in-house toolbox "Multi Physics Solver" MuPhyS (www.muphys.surfgroup.be, see e.g.,[35–37]). MuPhyS is a tool to solve physical and chemical systems, which can be expressed by a system of partial differential equations. Examples are flow simulations, elasticity problems, mechanical stress calculations, thermal problems, and many more.

We here emphasize that we interpret c_n as follows: According to Kilic and Bazant, c_n represents the concentration of the solvent, that is, an actual physical concentration for which a balance equation (that takes the form of a dilute solution balance equation) can be written, too. However, for such an interpretation, the local volume of the ions is calculated based on the local concentrations, which can only be done using atomistic simulations. Otherwise, we need to accept the assumption that the volumes of the ions in the solution are constant, irrespective of the composition of the solution. Thus, this point of view requires additional computational effort.

Therefore, we do not regard c_n as the concentration of a physical species, but instead, we regard v_n as the difference between the actual volume of the solution and the volume which the solution would occupy if the radius of every ion in the solution equaled the equivalent radius in an ionic crystal. Therefore, we interpret c_n as a measure for the nonideality of the solution:

- Large c_n indicates that the ions behave as if being in a perfectly dilute solution.
- $c_n \approx 0$ implies that the solution is so concentrated that every ion occupies only the space it would occupy in a crystal lattice.

- Negative c_n is physically impossible; it implies a region where concentrations are unrealistically high.

In addition, we consider the following homogeneous reactions

$$Me(H_2O)_4^{2+} + 2Cl^- \leftrightharpoons MeCl_2(H_2O)_4, \quad (33)$$

$$H^+ + OH^- \leftrightharpoons H_2O. \quad (34)$$

The rate coefficients of reactions (33) are calculated based on the imposed bulk concentrations and on Equation (17).

3 | RESULTS

3.1 | Spatial evolution of the species concentrations

We have simulated the motion and reaction of the species summarized in Table 2 with the DSM and with the SEM for current densities between 10^{-2} and 10^2 A cm^{-2}, which is also relevant for pitting corrosion at high current densities.[38–41]

Figure 2 compares the concentration profiles of H_2O, $Me(H_2O)_4$, Cl^-, and Na^+ as a function of x for the two

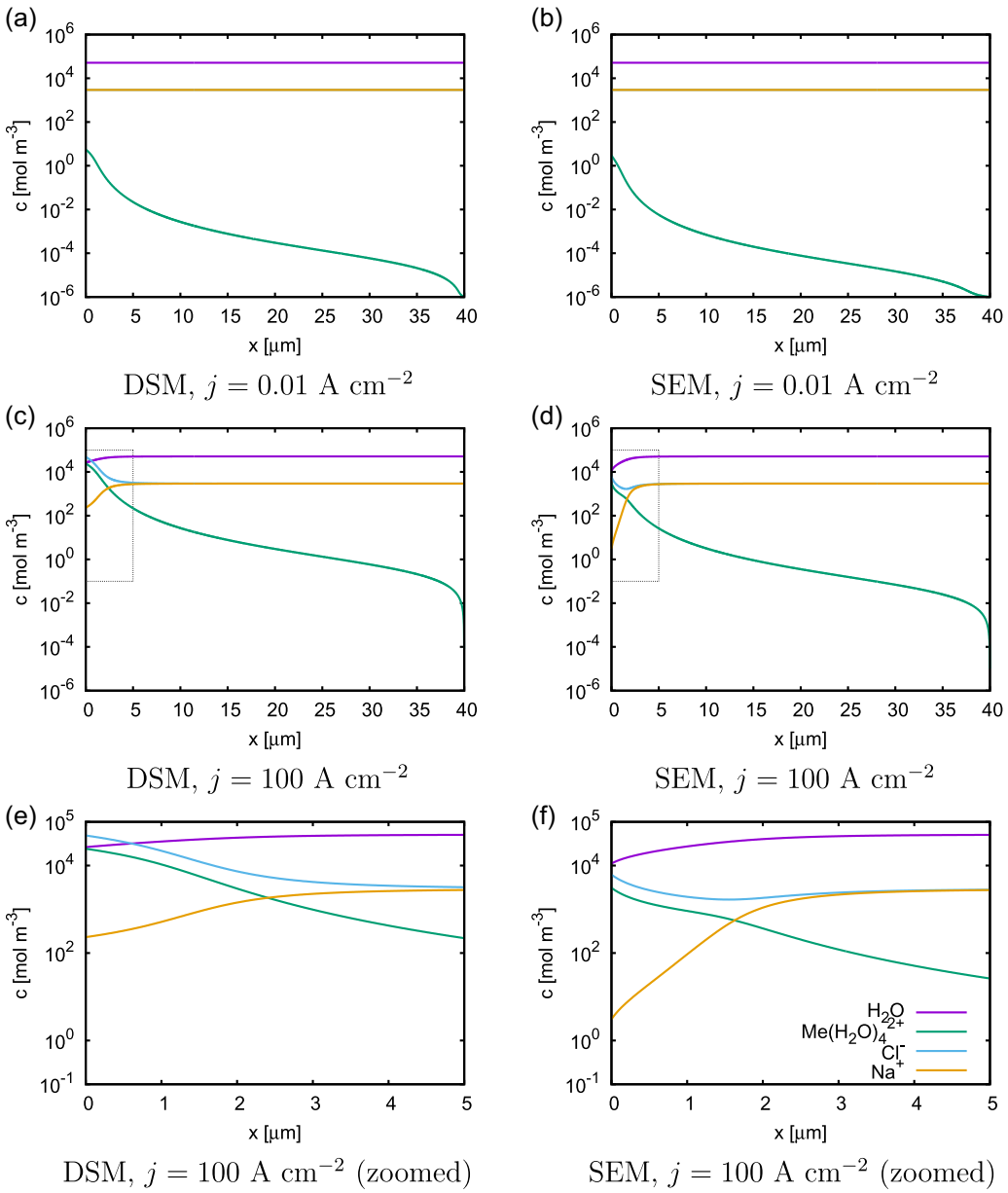

FIGURE 2 The concentrations of H_2O, $Me(H_2O)_4^{2+}$, Cl^-, and Na^+ for the dilute solution model (DSM; a,c,e) and the steric effect model (SEM, b,d,f) for $j = 0.01$ A cm^{-2} and $j = 100$ A cm^{-2}. The last row (e,f) zooms into the region indicated by the dotted box in the second row [Color figure can be viewed at wileyonlinelibrary.com]

different models for different current densities. In both models, we observe that the concentration of $Me(H_2O)_4^{2+}$ is increased at the boundary $x = 0$ and decreases away from the boundary. For low current densities, the influence of the SEM effects is negligible and the concentrations at the borders are almost identical. However, for large current densities (panels c and d, zoomed-in panels e and f) in the SEM model, the concentration of water at the boundary is reduced more significantly than in the DSM model, which we refer to as the "water-repelling" effect, resulting in an additional resistive layer. Consequently, there are also less hydrated $Me(H_2O)_4^{2+}$ ions.

Figure 3a,b shows the concentrations at the boundary $x = 0$ as a function of the current density in more detail. Panel c of the same figure shows the ratio of the concentrations between the SEM and the DSM model. Again, it shows that for small current densities, the concentration distributions are almost identical. However, at large current densities, the concentration of $Me(H_2O)_4^{2+}$, including steric effects, shows a clear limitation of the concentration close to the surface; in addition there is the reduction of water, which is the "water-repelling" effect mentioned above.

In both models, the sodium concentration is decreasing with increasing current density due to electroneutrality, where the metal ions are replacing the sodium ions. Also, the anion concentration increases to compensate for the metal ions and the water concentration decreases as water participates in the reactions. However, the SEM shows that the reduction of water concentration due to steric effects is more important than due to chemical reactions.

To extrapolate our results to even higher current densities, we have fitted different functions to the concentrations c as a function of the current densities using Gnuplot's nonlinear least-squares Marquardt–Levenberg algorithm. Table 3 gives an overview of the species and which function fits the boundary concentration best for both models. It illustrates that for both models, the concentrations of water and sodium ions behave approximately as an exponential function, whereas the concentration of chloride ions grows linearly and of $Me(H_2O)_4^{2+}$ grows as a power function.

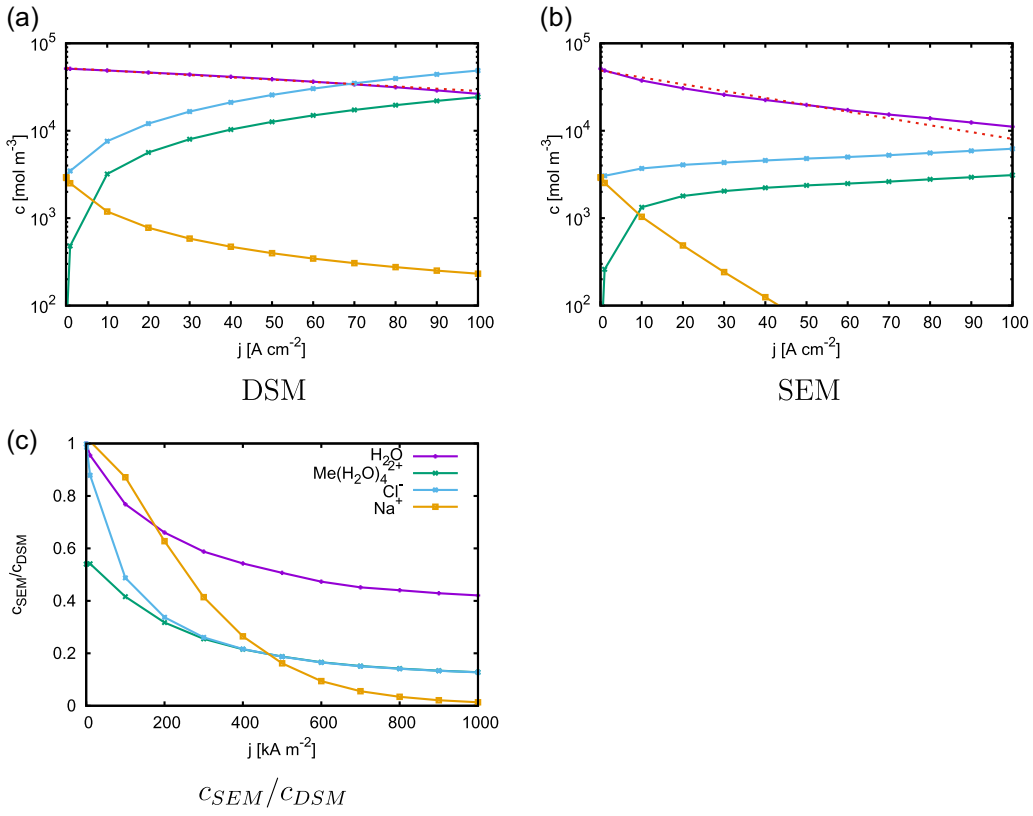

FIGURE 3 (a,b) The concentrations of the same species as in Figure 2 at the domain boundary $x = 0$ as a function of the current density j. The dotted red line shows the fit, summarized in Table 3, for water. (c) The ratio of the boundary concentrations for the steric effect model and the dilute solution model [Color figure can be viewed at wileyonlinelibrary.com]

Model	Species	Fit function c[mol m^{-3}]	A	b
DSM	H_2O	a × $e^{j\,[Acm^{-2}]\times b}$	$51{,}900 \pm 350$	$(-6 \pm 0.2) \times 10^{-3}$
DSM	$Me(H_2O)_4^{2+}$	a × j[Acm^{-2}]b	43 ± 2	10 ± 0.1
DSM	Cl^-	a × j[Acm^{-2}] + b	46 ± 0	$29{,}300 \pm 350$
DSM	Na^+	a × $e^{j[Acm^{-2}]\times b}$	$48{,}730 \pm 1290$	$(-2 \pm 0.1) \times 10^{-2}$
SEM	H_2O	a × $e^{j[Acm^{-2}]\times b}$	$48{,}730 \pm 1290$	$(-2 \pm 0.1) \times 10^{-2}$
SEM	$Me(H_2O)_4^{2+}$	a × j[Acm^{-2}]b	203 ± 33	4 ± 0.3
SEM	Cl^-	a × j[Acm^{-2}] + b	3 ± 0	$31{,}800 \pm 800$
SEM	Na^+	a × $e^{j[Acm^{-2}]\times b}$	2880 ± 30	$(-9 \pm 0.4) \times 10^{-2}$

TABLE 3 The applied fit function and fit values for the concentration c (a, b) [mol m^{-3}] of different species at the boundary $x = 0$ in different models

3.2 | Evolution of the electrostatic potential

Figure 4 shows the potential U in the electrolyte for the same cases as in Figure 2. Beyond $\approx 3\,\mu m$, the potential in all cases follows Ohm's law with a conductivity that corresponds to the bulk solution. The potential is comparable for the DSM and the SEM model because migration effects still dominate at the interface and thus the charged species are not influenced as much as the neutral particles. However, the influence of the applied current density is significant; the potential decreases everywhere with decreasing current density.

Figure 5 shows the boundary potential as a function of the current density. As we have already observed in Figure 4, the potential at the boundary decreases significantly with decreasing current density. In addition, the right y-axis of Figure 5 shows the ratio of the boundary potentials of the DSM and the steric effects model. Although the ratio decreases slightly with increasing current, it shows that for the cases considered here, there is no significant influence of taking into account the different sizes of the modeled species on the electrostatic potential.

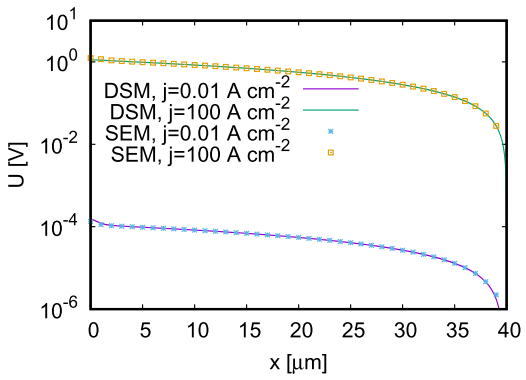

FIGURE 4 The potential as a function of position for the same models and current densities as in Figure 2 [Color figure can be viewed at wileyonlinelibrary.com]

4 | CONCLUSIONS AND OUTLOOK

In this study, we performed ECM simulations for different current densities with and without steric effects and analyzed such effects on the evolution of various species concentrations and on the electrostatic potential.

We have seen that for small current densities, there is no difference between the DSM and the SEM. However, the larger the current density becomes, the more significant the effect of the sizes of the different species becomes. For large current densities, water is repelled from the boundary and there are fewer $Me(H_2O)_4^{2+}$ ions at the boundary. We have seen that the boundary concentrations of the different species can be fitted with different functions: water and sodium ions with an exponential function, chloride ions with a linear function and $Me(H_2O)_4^{2+}$ with a power law, which gives us the means to extrapolate our results even for high current densities.

On the contrary, we have seen that the potential over the whole simulation domain is almost insensitive to the applied model and increases significantly with increasing current.

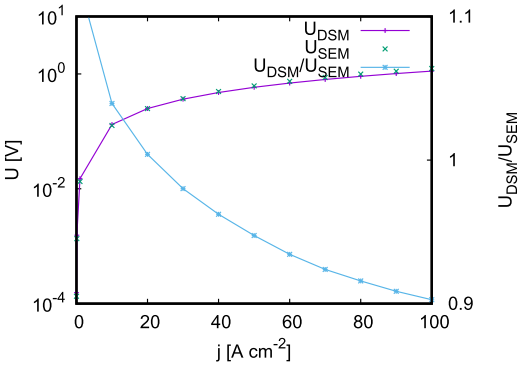

FIGURE 5 The potential at the boundary $x = 0$ as a function of the current density. The right y-axis shows the ratio of the two different models [Color figure can be viewed at wileyonlinelibrary.com]

Hence, steric effects can contribute significantly to electrochemical polishing as well as the ECM process with high current densities. For pitting or crevice corrosion, the preferred model depends really on the current densities. For standard processes with low current densities, the dilute system model is sufficient, whereas steric effects become important for gap lengths below 50 μm and high current densities as regarded in this article. Thus, conclusively, both models, DSM and SEM, have their relevance for different regimes: While DSM works well for processes with small current densities, it reaches its limits for high current densities and should be expanded through the SEM. The main limit of the presented model is the assumption of a constant ionic radius; the presented model is thus only applicable to solutions where the involved solutes approximately meet this requirement. But within the range of applicability, we would like to emphasize that simulations like the ones presented here are—in their limits—a dedicated tool to scan a parameter range (which might even be inaccessible by experiments) such as to calculate the dependence of the concentrations on the applied current (cf. Table 3).

The fact that no "water-repelling" function is needed to form the gel layer is an attractive aspect of steric effects. For those reasons, we suggest it to be worth to continue this line of research and use SEMs applying to the ECM process. In addition, future models dealing with steric effects should also be extended to include more realistic electrochemical systems.

Finally, we would like to emphasize that for realistic domain sizes and particle numbers; it might be more realistic to perform a series of 1D simulations to study steric effects on the anodic dissolution at high current densities and to derive from these results a macroscopic "water-repelling" function that is used in simpler models.

Although in theory, given the correct chemical reactions, molecular dynamics (MD) or Monte Carlo (MC) simulations tracing all individual particles, see for example,[42,43] might be used to study steric effects, this is currently not feasible because of the large number of involved particles. However, with the current development of computer power or of quantum computers,[44–47] the simulation of steric effects with MD or MC models might become feasible in the future.

ACKNOWLEDGMENTS

The authors would like to thank Michael Schneider from the Fraunhofer, IKTS Dresden, Germany, for fruitful discussions, which helped to improve the article.

DATA AVAILABILITY STATEMENT

Data available on request from the authors.

ORCID

Christoph Köhn http://orcid.org/0000-0002-7101-5889

REFERENCES

[1] A. D. Davydov, *J. Electrochem.* **2008**, *44*, 835.
[2] W. Han, F. Fang, *Int. J. Mach. Tools Manuf.* **2019**, *139*, 1.
[3] M. M. Lohrengel, K. P. Rataj, T. Münninghof, *Electrochim. Acta* **2016**, *201*, 345.
[4] M. Datta, *IBM J. Res. Dev.* **1993**, *37*, 207.
[5] M. Schneider, S. Schroth, S. Richter, S. Höhn, N. Schubert, A. Michaelis, *Electrochim. Acta* **2011**, *56*, 7628.
[6] M. Schneider, N. Schubert, S. Höhn, A. Michaelis, *Mater. Corros.* **2014**, *66*, 549.
[7] M. Schneider, N. Schubert, A. Michaelis, *Mater. Corros.* **2017**, *68*, 645.
[8] D. Landolt, P. F. Chauvy, O. Zinger, *Electrochim. Acta* **2003**, *48*, 3185.
[9] P. S. Kao, H. Hocheng, *J. Mater. Proc. Technol.* **2003**, *140*, 255.
[10] R. Mahdavinejad, M. Hatami, *J. Mater. Proc. Technol.* **2008**, *202*, 307.
[11] H. Luo, D. Mi, W. Nats, *Prec. Eng.* **2019**, *56*, 330.
[12] V. Kirchner, L. Cagnon, R. Schuster, G. Ertl, *Appl. Phys. Lett.* **2001**, *79*, 1721.
[13] W. Chen, F. Han, J. Wang, *Int. J. Adv. Manuf. Technol.* **2018**, *96*, 1367.
[14] B. H. Kim, C. W. Na, Y. S. Lee, D. K. Choi, C. N. Chu, *CIRP Ann.* **2005**, *54*, 191.
[15] Z. P. Zheng, W. H. Cheng, F. Y. Huang, B. H. Yan, *J. Micromech. Microeng.* **2007**, *17*, 960.
[16] D. Zhu, N. S. Qu, H. S. Li, Y. B. Zeng, D. L. Li, S. Q. Qian, *CIRP Ann.* **2009**, *58*, 177.
[17] J. Liu, C. Gao, L. Shen, H. Cheng, X. Gao, X. Han, *Int. J. Electrochem. Sci.* **2018**, *13*, 10654.
[18] M. M. Lohrengel, I. Kluppel, C. Rosenkranz, H. Bettermann, J. W. Schultze, *Electrochim. Acta* **2003**, *48*, 3203.
[19] M. Z. Bazant, M. S. Kilic, B. D. Storey, A. Ajdari, *Adv. Colloid Interface Sci.* **2009**, *152*, 48.
[20] J. E. Dykstra, P. M. Biesheuvel, H. Bruning, A. Ter Heijne, *Phys. Rev. E.* **2014**, *90*, 013302.
[21] Z. Du, H. Li, T. Gu, *Biotech. Adv.* **2007**, *25*, 464.
[22] H. V. M. Hamelers, A. Ter Heijne, T. H. J. A. Sleutels, A. W. Jeremiasse, D. P. Strik, C. J. N. Buisman, *Appl. Microbiol. Biotech.* **2010**, *85*, 1673.
[23] S. V. van Damme, G. Nelissen, B. V. D. Bossche, J. Deconinck, *J. Appl. Electrochem.* **2005**, *36*, 1.
[24] D. Deconinck, S. V. van Damme, J. Deconinck, *Electrochim. Acta* **2012**, *60*, 321.
[25] M. Purcar, L. Bortels, B. van den Bossche, J. Deconinck, *J. Mater. Proc. Technol.* **2004**, *149*, 472.
[26] D. Deconinck, S. van Damme, J. Deconinck, *Electrochim. Acta* **2012c**, *69*, 120.
[27] M. Kilic, M. Bazant, A. Ajdari, *Phys. Rev. E* **2007a**, *75*, 021501.
[28] M. Kilic, M. Bazant, A. Ajdari, *Phys. Rev. E* **2007b**, *75*, 021503.
[29] T. C. Lin, B. Eisenberg, *Commun. Math. Sci.* **2014**, *12*, 149.
[30] V. Kralj-Iglič, A. Iglič, *J. Phys. II* **1996**, *6*, 477.
[31] P. Perrot, *A to Z of Thermodynamics*, Oxford University Press, Oxford **1998**.
[32] H. Robbins, *Am. Math. Month.* **1955**, *62*, 26.

[33] O. Dolgikh, A. S. Demeter, A. C. Bastos, V. Topa, J. Deconinck, *Electrochem. Commun.* **2013**, *37*, 20.
[34] S. van Damme, G. Nelissen, B. van den Bossche, J. Deconinck, *J. Appl. Electrochem.* **2006**, *36*, 1.
[35] D. Deconinck, *Ph.D. Thesis*, VU Brussels, Belgium, **2012**.
[36] E. Hotoiu, S. van Damme, C. Albu, D. Deconinck, A. Demeter, J. Deconinck, *Electrochim. Acta* **2013**, *93*, 8.
[37] T. Muselle, H. Simillion, D. van Laethem, J. Deconinck, A. Hubin, *Electrochim. Acta* **2017**, *245*, 173.
[38] P. Poyet, A. Desestret, H. Corious, L. Grall, *Mem. Sci. Rev. Metall.* **1975**, *72*, 133.
[39] R. Doelling, K. E. Heusler, *Z. f. Phys. Chem.* **1984**, *139*, 39.
[40] L. I. Frejman, Y. Flis, M. Prazhak, *Electrochem. tests Z. Metal.* **1986**, *22*, 179.
[41] E. Otero, J. Botella, J. Botana, V. Matres, R. Merello, *Rev. de Metal.***2005**, *41*, 148.
[42] M. H. Mamme, C. Köhn, J. Deconinck, J. Ustarroz, *Nanoscale* **2018**, *10*, 1039.
[43] C. Köhn, M. B. Enghoff, H. Svensmark, *J. Comp. Phys.* **2018**, *363*, 30.
[44] G. Moore, *Electronics* **1965**, *38*, 114.
[45] M. Waldrop, *Nature* **2016**, *530*, 144.
[46] M. Mohseni, P. Read, H. Neven, S. Boixo, V. Denchev, R. Babbush, A. Fowler, V. Smelyanskiy, J. Martinis, *Nature* **2017**, *543*, 171.
[47] F. Arute, K. Arya, R. Babbush, D. Bacon, J. C. Bardin, R. Barends, R. Biswas, S. Boixo, F. Brandao, D. A. Buell, B. Burkett, Y. Chen, Z. Chen, B. Chiaro, R. Collins, W. Courtney, A. Dunsworth, E. Farhi, B. Foxen, A. Fowler, C. Gidney, M. Giustina, R. Graff, K. Guerin, S. Habegger, M. P. Harrigan, M. J. Hartmann, A. Ho, M. Hoffmann, T. Huang, T. S. Humble, S. V. Isakov, E. Jeffrey, Z. Jiang, D. Kafri, K. Kechedzhi, J. Kelly, P. V. Klimov, S. Knysh, A. Korotkov, F. Kostritsa, D. Landhuis, M. Lindmark, E. Lucero, D. Lyakh, S. Mandrà, J. R. McClean, M. McEwen, A. Megrant, X. Mi, K. Michielsen, M. Mohseni, J. Mutus, O. Naaman, M. Neeley, C. Neill, M. Y. Niu, E. Ostby, A. Petukhov, J. C. Platt, C. Quintana, E. G. Rieffel, P. Roushan, N. C. Rubin, D. Sank, K. J. Satzinger, V. Smelyanskiy, K. J. Sung, M. D. Trevithick, A. Vainsencher, B. Villalonga, T. White, Z. J. Yao, P. Yeh, A. Zalcman, H. Neven, J. M. Martinis, *Nature* **2019**, *574*, 505.

How to cite this article: Köhn C, van Laethem D, Deconinck J, Hubin A. A simulation study of steric effects on the anodic dissolution at high current densities. *Materials and Corrosion*. 2021;72:610–619. https://doi.org/10.1002/maco.202012051